

# Dynamics of Hydrogen in Silicon at Finite Temperatures from First Principles

Diana Gomes, Vladimir P. Markevich, Anthony R. Peaker, and José Coutinho\*

Hydrogen defects in silicon still hold unsolved problems, whose disclosure is fundamental for future advances in Si technologies. Among the open issues is the mechanism for the condensation of atomic hydrogen into molecules in Si quenched from above  $T \approx 700^\circ\text{C}$  to room temperature. Based on first-principles calculations, the thermodynamics of hydrogen monomers and dimers is investigated at finite temperatures within the harmonic approximation. Free energies of formation indicate that the population of  $\text{H}^-$  cannot be neglected when compared to that of  $\text{H}^+$  at high temperatures. The results allow us to propose that molecular formation occurs during cooling processes, in the temperature window  $T \approx 700 - 500\text{ K}$ , above which the molecules collide with Si—Si bonds and dissociate, and below which the fraction of  $\text{H}^-$  becomes negligible. The formation of  $\text{H}^-$  and most notably of a fast-diffusing neutral species can also provide an explanation for the apparent accelerated diffusivity of atomic hydrogen at elevated temperatures in comparison to the figures extrapolated from measurements carried out at cryogenic temperatures. Finally, it is shown that the observed diffusivity of molecules is better described upon the assumption that they are nearly free rotors, all along the migration path, including at the transition state.

## 1. Introduction

The presence of hydrogen in crystalline silicon is almost unavoidable. H species are highly mobile and reactive; they can change several properties of the host upon interactions with point and extended defects, as well as with contaminants and dopants. Hydrogen is employed on wafer processing and surface treatments; it is determinant in the performance of oxide–semiconductor interfaces, and for these and many other reasons, few are the elements that deserved so much attention in the past

60 years or so of research of defects in silicon.<sup>[1–4]</sup> The current understanding of hydrogen point defects in Si has been recently reviewed,<sup>[5,6]</sup> both from the experimental and theoretical perspectives. We only summarize the essential features for the sake of the present work.

From electron paramagnetic resonance,<sup>[7–9]</sup> deep-level transient spectroscopy (DLTS),<sup>[10,11]</sup> Fourier transform infrared absorption spectroscopy,<sup>[12]</sup> muon spin rotation spectroscopy,<sup>[13]</sup> and theoretical modeling,<sup>[14–19]</sup> there is ample evidence and reasoning for the presence of isolated hydrogen atoms and ions in Si. Atomic H can trap a hole to become a proton located at the bond-centered site ( $\text{H}_{\text{BC}}^+$ ). It can also trap one electron to become a hydride ion which, according to theorists, finds its most stable state in the open regions of the lattice, either at the tetrahedral interstitial site ( $\text{H}_{\text{T}}^-$ ),<sup>[15,17,19]</sup> or, close to it, at the antibonding site ( $\text{H}_{\text{AB}}^-$ ).<sup>[14,16,20]</sup> This ambiguity reflects the shallowness of the potential energy for the roaming of  $\text{H}^-$  within the

volume enclosed by the tetrahedral cage of the Si lattice.<sup>[19]</sup> The above crystalline sites are represented in **Figure 1**.


Single hydrogen atoms in Si show negative-*U* properties and bistability in the neutral charge state.<sup>[10]</sup> Essentially,  $\text{H}^0$  is metastable against disproportionation,  $2\text{H}^0 \rightarrow \text{H}^+ + \text{H}^-$ .<sup>[21,22]</sup> This is clearly understood if we break the reaction into two steps, and realize that the small ionization energy for  $\text{H}_{\text{BC}}^0 \rightarrow \text{H}_{\text{BC}}^+ + e^-$  (0.175 eV) is overcompensated by the affinity for  $\text{H}_{\text{BC}}^0 + e^- \rightarrow \text{H}_{\text{T}}^-$  (estimated between  $-0.4$  and  $-0.6$  eV).<sup>[11,23]</sup> Importantly, because only the metastable  $\text{H}_{\text{T}}^0$  state can become negatively charged, the second step includes a reconfiguration barrier of  $\approx 0.3$  eV involving  $\text{H}_{\text{BC}}^0 \rightarrow \text{H}_{\text{T}}^0$  that must be surmounted.<sup>[11]</sup> This barrier explains why H at the BC site is the dominant species found in low-temperature proton-implanted n-type Si,<sup>[7,8]</sup> despite the fact that under these conditions the ground state is  $\text{H}_{\text{T}}^-$  (or  $\text{H}_{\text{AB}}^-$ ). The above picture implies that atomic H has a  $(-/+)$  occupancy level in the range 0.3–0.4 eV below the conduction band bottom ( $E_{\text{c}}$ ), with the uncertainty arising from difficulties in measuring the energy of  $\text{H}_{\text{T}}^0$  with respect to  $\text{H}_{\text{BC}}^0$ .<sup>[23]</sup>

It is also very hard to measure the diffusivity of hydrogen without the result being affected by impurity trapping (dopants, oxygen, and carbon, to name some of the most important). Two experiments that avoided this effect are highlighted. In a 1996 article, the decay rate of a stress-aligned population of  $\text{H}_{\text{BC}}^+$

D. Gomes, J. Coutinho  
I3N

Department of Physics  
University of Aveiro  
Campus Santiago, 3810-193 Aveiro, Portugal  
E-mail: jose.coutinho@ua.pt

V. P. Markevich, A. R. Peaker  
Photon Science Institute and Department of Electrical and Electronic Engineering  
The University of Manchester  
Manchester M13 9PL, UK

 The ORCID identification number(s) for the author(s) of this article can be found under <https://doi.org/10.1002/pssb.202100670>.

DOI: 10.1002/pssb.202100670

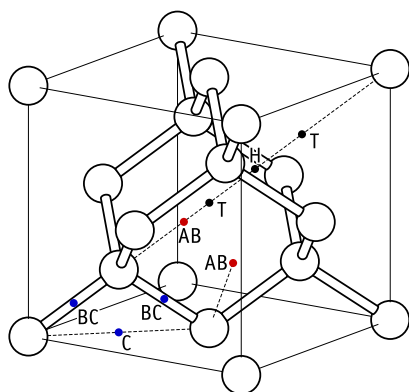


**Figure 1.** Conventional cell of silicon. High symmetry crystalline sites are indicated with dots along with (commonly used) labels. The coloring of dots is helpful for the discussion of migration and reorientation mechanisms of hydrogen defects in different charge states.

defects was measured during annealing in the temperature range  $T = 126 - 142$  K by Gorelinskii and Nevynnyi (GN).<sup>[8]</sup> The result,  $\nu = (2.3 \text{ THz}) \exp(-0.43 \pm 0.02 \text{ eV} / k_B T)$ , was interpreted as reflecting the jump of individual protons between neighboring bond-centered sites during the return to natural randomness. The pre-exponential factor is consistent with a phonon activated single jump. Following Herring et al.,<sup>[17]</sup> we can convert the measured dichroism decay rate,  $\nu$ , into diffusivity as  $D = l^2 \nu / 8$ , which gives  $D = (1.06 \times 10^{-4} \text{ cm}^2 \text{ s}^{-1}) \exp(-0.43 \pm 0.02 \text{ eV} / k_B T)$ , where we considered the distance between neighboring bond-centered sites  $l = 1.92 \text{ \AA}$  as the elementary jump length. In the other experiment, published in 1956, the escape of pressurized molecular hydrogen through thin-walled Si canisters was monitored by Van Wieringen and Warmoltz (VWW) in the temperature range  $T = 1090 - 1200$  °C.<sup>[24]</sup> At such high temperatures, trapping processes become insignificant, and a diffusivity  $D = (9.4 \times 10^{-3} \text{ cm}^2 \text{ s}^{-1}) \exp(-0.48 \pm 0.05 \text{ eV} / k_B T)$  was found. From the pressure dependence of the hydrogen permeation, it was clear that hydrogen migrated in the atomic form. Considering the close activation energies extracted from the low- and high-temperature data, it is commonly assumed that transport of atomic hydrogen in Si occurs via consecutive jumps of  $\text{H}^+$  between neighboring bond-centered sites.

Among the many measurements of the hydrogen diffusivity close to room temperature (see Peaker et al.<sup>[5]</sup> for a collection of data), the one of Kamiura, Yoneta, and Hashimoto (KYH)<sup>[25]</sup> falls distinctively close to the line that connects the VWW and GN data points. In this work, the in-diffusion kinetics of H released from photoinduced dissociation of carbon–hydrogen complexes near the surface of the silicon (formed via wet-etching) was measured in the range  $T = 220 - 270$  K, leading to a diffusivity  $D = (7 \times 10^{-2} \text{ cm}^2 \text{ s}^{-1}) \exp(-0.54 \text{ eV} / k_B T)$ . This result was claimed to reflect a rate-limiting process involving the diffusion of hydrogen to phosphorous atoms.<sup>[25]</sup>

Hydrogen in Si is also found in the form of pairs. At least two H dimers were found experimentally in the Si lattice, namely, the hydrogen molecule located at the tetrahedral interstitial site ( $\text{H}_{2\text{T}}$ ) and a close pair of  $\text{Si}-\text{H}_{\text{BC}} \cdots \text{Si}-\text{H}_{\text{AB}}$  units, referred to as  $\text{H}_2^+$ .

While in very pure Si, the molecule can represent the main stock of free hydrogen available at room temperature,<sup>[26]</sup>  $\text{H}_2^+$  has been mostly detected in irradiated material,<sup>[27]</sup> despite having a formation energy of only few tenths of eV higher than the molecule.<sup>[28]</sup> Formation of  $\text{H}_2^+$  in nonirradiated Si has also been reported by Suezawa though.<sup>[29]</sup> A possible route for its formation has been proposed by Estreicher et al.,<sup>[30]</sup> and involves the interaction of  $\text{H}_2$  molecules with radiation-induced defects.

From a reinterpretation of the outdiffusion kinetics of tritium quenched samples,<sup>[31]</sup> the existence of a third and nondetectable hydrogen dimer, referred to as  $\text{H}_{2\text{B}}$ , has been postulated by Voronkov and Falster.<sup>[32]</sup> This species would account for the difference in the concentration of hydrogen–boron complexes (HB) formed after complete conversion of  $\text{H}_{2\text{T}}$  molecules into HB in boron-doped material annealed at 160 and 175 °C. Assuming that  $\text{H}_{2\text{B}}$  is not stable at the higher temperature, its dissociation would explain the observation of a 45% increase in the formation of HB pairs.

Although being electrically inert,  $\text{H}_{2\text{T}}$  molecules can be detected by local vibrational mode (LVM) spectroscopy, either via Raman scattering or absorption in the infrared region.<sup>[27,33,34]</sup> They can be introduced in Si upon exposing the material to a low-temperature ( $\approx 150$  °C) hydrogen plasma<sup>[33]</sup> or to a high-temperature ( $T \gtrsim 700$  °C) gas phase followed by quenching. In the latter case, concentrations of interstitial molecules of a few times  $10^{15} \text{ cm}^{-3}$  could be reached.<sup>[34]</sup> The molecules become mobile above 30 °C, and can be trapped by/near impurities such as interstitial oxygen ( $\text{O}_i$ ),<sup>[35]</sup> substitutional carbon,<sup>[36]</sup> or substitutional boron.<sup>[37]</sup> From the dissociation/recovery kinetics of  $\text{O}_i-\text{H}_2$ , a diffusivity  $D = (2.6 \pm 1.5 \text{ cm}^2 \text{ s}^{-1}) \times 10^{-4} \exp(-0.78 \pm 0.05 \text{ eV} / k_B T)$  was attributed to the migration of  $\text{H}_2$  across the Si lattice.<sup>[35]</sup>

Despite the success in predicting and describing the properties of H-related point defects by first-principles methods, including their vibrational and electronic properties,<sup>[36,38–40]</sup> several issues were left unsolved. Among the fundamental problems, the most intriguing is perhaps the mechanism for the formation of  $\text{H}_2$  molecules from atomic hydrogen upon cooling the crystals from high temperatures. The main difficulty is that the Fermi level is close to midgap and with the  $(-/+)$  level of hydrogen at 0.3–0.4 eV below  $E_c$ , the population of H monomers is thought to consist essentially of mutually repelling  $\text{H}^+$  ions.

The migration of hydrogen also has open issues. As pointed out in the study by Voronkov and Falster,<sup>[41]</sup> if we extrapolate the diffusivity from the low-temperature data to the range of the high-temperature experiment, the diffusivity obtained for  $\text{H}^+$  is several times lower than that recorded by VWW. It was then suggested that neutral hydrogen, although present in small quantities, could dominate the diffusivity at high temperatures due to its low migration barrier.<sup>[32,41]</sup> Despite its significance, this observation is based on a rather extreme extrapolation spanning 17 orders of magnitude of diffusivity, between the high-temperature data of VWW,<sup>[24]</sup> which covered a narrow range of only a factor of two, and the low-temperature data of GN<sup>[8]</sup> obtained over two decades.

Another issue is the migration barrier of  $\text{H}^-$  which has been calculated as 0.39 eV,<sup>[19]</sup> nearly half of the value (0.7 eV) obtained from the kinetics of hydrogen passivation/reactivation of phosphorous donors.<sup>[42]</sup> A possible solution for

this discrepancy involves an alternative interpretation of the measured 0.7 eV barrier, which would correspond to a reorientation of the P–H complex accompanied by a charge state change.<sup>[43]</sup> The neutral state is even more puzzling—the barrier for migration between  $H_{BC}^0$  ground states has a calculated value of 0.38 eV.<sup>[19]</sup> No measurements are available for this figure, essentially because of the short lifetime of neutral hydrogen. However, a striking observation was that upon forward-bias injection of  $p^+-n$  diodes at 65 K,<sup>[11]</sup> when most hydrogen atoms were assumed to be in the metastable neutral state (referred to as  $H_T^0$ ), the estimated diffusivity was 27 orders of magnitude higher compared to that of  $H^+$  at the same temperature as extrapolated from the VWW data.<sup>[24]</sup> If we accept such an extrapolation as meaningful (based on data that span less than a decade of diffusivity), it suggests that there is a barrier preventing the relaxation  $H_T^0 \rightarrow H_{BC}^0$ , which must be higher than the barrier for migration between  $H_T^0$  states, and the latter should be lower than 0.1 eV.<sup>[23]</sup>

A rather impactful problem involving hydrogen in silicon is light- and elevated temperature-induced degradation (LeTID) of silicon solar cells.<sup>[44]</sup> This effect is responsible for a decrease of the power conversion efficiency of modules by up to 16% relative, and it was found to be particularly detrimental in new-generation multicrystalline passivated emitter and rear cells (see Chen et al.<sup>[45]</sup> for a recent review). Based on junction spectroscopy and first-principles calculations, the relocation of hydrogen and the formation of a boron–dihydride complex ( $BH_2$ ) in p-type Si has been proposed as a possible culprit for LeTID.<sup>[46]</sup>

The understanding of LeTID is strongly tied with our knowledge regarding the issues discussed above. They involve processes driven by kinetics and excitations (quenching, illumination, annealing), all of which cannot be understood if we leave vibrational and electronic excitations out of the physical picture. The recent work by Sun and co-workers<sup>[47,48]</sup> revised the second (electronic) type of excitations, with an evaluation of the relative concentrations of different charge states of H under nonequilibrium steady-state carrier injection. In this article, we consider the effect of vibrational degrees of freedom on several hydrogen-related properties and processes.

The next sections are organized as follows: Section 2 describes the methodology, including the calculation of electronic plus clamped ion energies, free energies of formation, activation energy barriers, reaction rates, and diffusion coefficients. The bulk of the results are described in Section 3. Along the way, we will 1) present a fresh look into the configuration coordinate diagram (CCD) of atomic H, describing carrier trapping/emission, as well as transformation and migration processes; 2) discuss a mechanism for the formation of molecules in quenched samples; and 3) reconcile the low-temperature measurements of the jump rate of  $H_{BC}^+$  with the high-temperature diffusivity. The article includes a table summarizing the main results and assignments along with several concluding remarks.

## 2. Methodology

### 2.1. All-Electron Energies

All-electron energies were calculated within density functional theory employing the plane-wave pseudopotential formalism.<sup>[49–52]</sup>

Either a semilocal density functional (generalized gradient approximation [GGA]<sup>[53]</sup>) or a range-separated hybrid functional (as proposed by Heyd, Scuseria, and Ernzerhof [HSE]<sup>[54,55]</sup>) described the electronic exchange–correlation interactions. The projector-augmented wave method was used to treat the core electrons,<sup>[56]</sup> whereas valence states were described by plane waves. The self-consistent electron density and potential were converged until the total energy between two consecutive steps differed by less than  $10^{-8}$  eV.

Several hydrogen defects were investigated. As for hydrogen monomers, the sites investigated are identified in the conventional unit cell of Si depicted in Figure 1. The usual labels are used for the bond-centered, antibonding, tetrahedral, and hexagonal (H) interstitial sites. Site C is also included for the sake of discussing migration and reorientation mechanisms. The different coloring of the dots also serves that purpose.

Two kinds of hydrogen dimers were investigated with particular detail, namely, the molecule at the T site,  $H_{2T}$ , and the  $H_2^*$  complex. The latter is made of neighboring  $H_{BC}$  and  $H_{AB}$  along the principal diagonal of the cube represented as a dashed line in Figure 1.

Three batches of first-principles calculations were carried out, namely, 1) total energy of stable structures; 2) minimum energy paths and respective energy barriers between stable structures; and 3) vibrational mode frequencies.

In type (1) calculations, the stable geometries of defects and respective energies were found in cubic supercells of 512 Si atoms with the plane-wave cutoff energy set to  $E_{\text{cut}} = 400$  eV. The Kohn–Sham problem was solved at  $\mathbf{k} = \Gamma$  only. Structural optimization (within GGA level) ensured that the residual forces acting on the nuclei were lower than  $0.01 \text{ eV } \text{\AA}^{-1}$ . A self-consistent calculation within HSE level was performed to evaluate the electronic energy of the periodic supercell,  $\tilde{E}_{\text{elec}}$ . Finally, a periodic charge correction was added to  $\tilde{E}_{\text{elec}}$  in order to find the (clamped ion) electronic energy of the defective cell,  $E_{\text{elec}} = \tilde{E}_{\text{elec}} + E_{\text{corr}}$ .<sup>[57]</sup>

In type (2) calculations, defect migration, reorientation, and transformation mechanisms were investigated by finding minimum energy paths using the climbing image nudged elastic band (NEB) method.<sup>[58]</sup> Accordingly, 11 intermediate structures between the initial and final states were relaxed while subject to the elastic band constraint. For that, we employed 64-atom cubic cells,  $E_{\text{cut}} = 400$  eV, a grid of  $2 \times 2 \times 2$   $\mathbf{k}$ -points for sampling the Brillouin zone, and the GGA exchange–correlation functional. Hybrid density functional single-point calculations were finally carried out in order to find the electronic component for the activation energy barrier  $\Delta E_{a,\text{elec}} = E_{\text{elec}}^\ddagger - E_{\text{elec}}$ , where  $E_{\text{elec}}^\ddagger$  and  $E_{\text{elec}}$  are HSE-level energies of the transition state and initial state, respectively.

In type (3) calculations, we constructed the dynamical matrix from the force constants  $\Phi_{ij} = -\partial F_i / \partial x_j$  using numerical differentiation with atomic displacements  $\Delta x = 0.01 \text{ \AA}$ . Here,  $\{i, j\} = 1, \dots, 3N$ ,  $F_i$  is a force component along  $i$ ,  $x_j$  is an atomic displacement along  $j$ , and  $N$  is the total number of atoms in the supercell. The dynamical matrix elements were found at  $\mathbf{q} = \Gamma$ . Harmonic vibrational mode frequencies were found via matrix diagonalization. These calculations were performed at the GGA level with  $E_{\text{cut}} = 500$  eV; the respective equilibrium

structures were found in  $N = 64$  atom supercells; residual forces of the relaxed structures were lower than  $0.005 \text{ eV } \text{\AA}^{-1}$ ; and a grid of  $2 \times 2 \times 2$   $k$ -points was used for BZ integration.<sup>[59]</sup> Convergence of the vibrational properties due to finite size effects was verified using larger 216 atom cells. Further testing has been reported elsewhere.<sup>[28,60]</sup>

## 2.2. Free Energies of Formation

The vast majority of experiments related to defects in silicon are performed at constant pressure. Therefore, quantities that are probed under thermodynamic equilibrium conditions relate to the (change in the) Gibbs free energy,  $\Delta G$ . On the other hand, from the perspective of modeling, it is convenient to work under constant volume and calculate changes in the Helmholtz free energy,  $\Delta F$ .<sup>[61,62]</sup> While for sufficiently large supercells, the potential contributions to the free energy (stationary ionic and electronic solutions) converge to the same value under constant pressure and constant volume regimes;<sup>[63]</sup> the same is not true for the vibrational free energy, which, being affected by anharmonicity, induces a ( $T$ -dependent) macroscopic volume change to the crystal. However, as pointed out by Estreicher et al.,<sup>[28]</sup> the minute thermal expansion of crystalline Si indicates that phonon frequencies change weakly with  $T$ , and that constant volume and constant pressure calculations are comparable up to a few hundred degrees Celsius. This is an important observation which is also assumed by us, although it should be taken with due care by the reader.

Regarding the calculation of the free energy of formation of defects in crystals, the formalism can be found elsewhere.<sup>[28,60,64]</sup> Here, we leave a summary of the main ingredients and approximations considered. Our starting point is a sample made of  $N_L$  lattice sites spanning, a constant volume  $V$ , and containing  $n_d$  defects. We assume a dilute limit, that is, the concentration of defects under scrutiny is low enough so that we can 1) ignore defect-defect interactions, including in the calculation of configurational entropy, and 2) neglect their impact on the location of the Fermi level. Accordingly, we can define the Helmholtz free energy of formation of a defective sample as

$$\Delta F_f = F - F^{(0)} \quad (1)$$

where  $F$  is the total free energy enclosed in the volume  $V$ , which includes potential terms as well as temperature-dependent excitations and entropy. Here, we consider electronic, vibrational, rotational (for the case of molecular  $\text{H}_2$  in Si), and configurational degrees of freedom

$$F = F_{\text{elec}} + F_{\text{vib}} + F_{\text{rot}} - TS_{\text{conf}} \quad (2)$$

The quantity  $F^{(0)}$  is a reference free energy which is further detailed below. The first term in Equation (2) accounts for the electronic (clamped ion) internal energy and entropy,  $F_{\text{elec}} = U_{\text{elec}} - TS_{\text{elec}}$ . However, for defects with deep gap states,  $F_{\text{elec}}$  is usually replaced by the zero-temperature internal energy,  $U_{\text{elec}}(T = 0\text{K}) = E_{\text{elec}}$ . The reason is that 1) the fraction of defects that can be promoted to electronic excited states drops exponentially with the excitation energy, and 2) the electronic entropy is proportional to the electronic density of states within

$E_F \pm k_B T$ , where  $E_F$  and  $k_B$  are the Fermi level and the Boltzmann constant, respectively.<sup>[65]</sup>

Estreicher et al.<sup>[28]</sup> showed that the electronic entropy of defects with states deeper than  $\approx 0.1 \text{ eV}$  from the band edges contributes no more than few tens of meV to the free energy, even for defect concentrations as high as  $10^{17} \text{ cm}^{-3}$  at  $T \approx 900 \text{ K}$ . Considering that H monomers are the only electronically active defects being investigated, and that the shallowest state to be considered is at  $\approx E_c - 0.2 \text{ eV}$ , we can safely assume that  $F_{\text{elec}} = E_{\text{elec}}$ , which is the ground state energy of the all-electron (plus nuclear) stationary solution of the problem, here obtained from a hybrid functional calculation as described in Section 2.1.

The vibrational free energy of  $3N - 3$  independent oscillators with frequency  $\omega_i$  involving  $N$  atoms is

$$F_{\text{vib}} = k_B T \sum_{i=1}^{3N-3} \log \left[ 2 \sinh \left( \frac{\hbar \omega_i}{2k_B T} \right) \right] \quad (3)$$

where  $\hbar$  is the reduced Plank constant. Equation (3) already includes the zero-point vibrational energy,  $E_{\text{ZP}} = \sum_i^{3N-3} \hbar \omega_i / 2$ , which along with the electronic component defines the potential energy of the problem  $E = E_{\text{elec}} + E_{\text{ZP}}$ . The vibrational frequencies,  $\omega_i$ , were obtained as described at the end of Section 2.1. The vibrational entropy and specific heat (at constant volume) are readily found from

$$S_{\text{vib}} = -\frac{\partial F_{\text{vib}}}{\partial T}; \quad c_v = -T \left( \frac{\partial^2 F_{\text{vib}}}{\partial T^2} \right) \quad (4)$$

**Figure 2** depicts the calculated specific heat at constant volume of bulk silicon, obtained from 189 vibrational frequencies of a 64-atom supercell (thick black line). In the same graph, we reproduce specific heat data measured at constant pressure.<sup>[66,67]</sup>

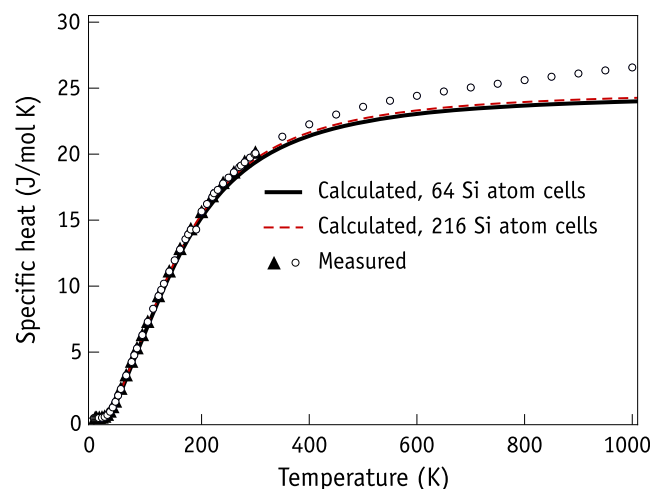


**Figure 2.** Specific heat of silicon. Circles and triangles represent data measured at constant pressure conditions,  $c_p$ , and reported in previous studies.<sup>[66,67]</sup> The two lines represent the calculated specific heat at constant volume,  $c_v$ , within the harmonic approximation (Equation (3) and (4)) using 189 vibrational frequencies from a 64-atom supercell (black thick line), and 645 vibrational frequencies from a 216-atom supercell (red dashed thin line).



Clearly, the calculation describes the measurements reasonably well up to a few hundred degrees K. This provides us an indication of the temperature beyond which the harmonic approximation starts to break. Above 400–600 K, anharmonic effects become sizable, i.e., for each vibrational mode, the energy separation between consecutive excited states decreases with increasing the temperature. Hence, beyond these thresholds, finite temperature calculations become more qualitative.

Also shown in Figure 2 is the specific heat calculated using a cubic supercell made of 216 Si atoms, corresponding to  $3N - 3 = 645$  vibrational frequencies (red dashed line). Clearly, the difference from the results using the smaller 64-atom cell is not substantial, suggesting that the sampling of the vibrational structure cannot be significantly improved by increasing the cell size.

In the dilute limit, all contributions to the free energy are extensive with respect to the number of defects. However, the configurational entropy,  $S_{\text{conf}}$ , is a nonlocal quantity that must be obtained from combinatorial analysis of all defect configurations across the whole sample volume. Accordingly, the number of distinct ways a population of  $n_d$  identical defects can be distributed over  $N_L$  lattice sites is

$$W = \frac{g^{n_d} N_L!}{(N_L - n_d)! n_d!} \approx \frac{(g N_L)^{n_d}}{n_d!} \quad (5)$$

where  $g$  is the number of degenerate orientations that each defect can have per lattice site. From the definition of entropy,  $S = k_B \log W$ , we can obtain an approximate expression for  $S_{\text{conf}}$  per defect after using a first-order Taylor's series for  $e^x$  and Stirling's formula

$$S_{\text{conf}} = k_B \left( 1 - \log \frac{c}{g} \right) \quad (6)$$

where  $c = n_d / N_L$  is the defect concentration.

Additional degrees of freedom can be added to Equation (2), depending on the specificity of the problem at hand. For instance, molecular hydrogen in Si essentially behaves as a free rigid rotor in the tetrahedral interstitial site.<sup>[68]</sup> To account for the thermal population of the rotational states, a rotational free energy contribution ( $F_{\text{rot}}$ ) must be considered

$$F_{\text{rot}} = -k_B T \log(Z_{\text{rot}}) \quad (7)$$

where  $Z_{\text{rot}} = Z_o^g Z_p^g$  is the rotational partition function obtained as a factorization of independent partition functions of ortho ( $Z_o$ ) and para ( $Z_p$ )  $\text{H}_2$  molecules, with respective naturally occurring fractions,  $g_o = 3/4$  and  $g_p = 1/4$ , reflect the degeneracy of each spin-isomer,<sup>[28,68–70]</sup> and

$$Z_{\{o,p\}} = \sum_{j=\{\text{odd, even}\}} (2j+1) \exp[-j(j+1)\theta_{\text{rot}}/T]. \quad (8)$$

In Equation (8), the index  $j$  either runs over odd or even integers for ortho- or para- $\text{H}_2$ , respectively, and the characteristic rotational temperature of interstitial  $\text{H}_2$  in Si is  $\theta_{\text{rot}} = 73.0$  K.<sup>[28]</sup>

We return now to the reference free energy  $F^{(0)}$  in Equation (1). This is usually broken into contributions from all  $n_i$  elements of species  $i$  enclosed within a sample volume,  $F^{(0)} = \sum_i n_i \mu_i^{(0)}$ .

Here,  $\mu_i^{(0)} = \partial F_i^{(0)} / \partial n_i$  is the chemical potential of the  $i$ th species, obtained from the free energy,  $F_i^{(0)}$ , of a reservoir usually considered under normal temperature and pressure conditions. We are only interested in the calculation of quantities that involve the conservation of chemical species, including electronic levels, binding energies, and energy barriers, all of which are independent of our choice for the chemical potentials. Therefore, we simply set  $\mu_{\text{Si}}^{(0)}$  to the free energy per atom in crystalline silicon at  $T = 0$  K, which includes electronic plus ionic and zero-point vibrational energies. As for  $\mu_{\text{H}}^{(0)}$ , it is found from the free energy per H atom in molecular  $\text{H}_2$  located at the tetrahedral interstitial site of silicon at  $T = 0$  K, i.e.,  $F = 2\mu_{\text{H}}^{(0)} + n_{\text{Si}}\mu_{\text{Si}}^{(0)}$ . This choice allows us to directly find the potential energy of a H defect with respect to the molecular state.

Atomic hydrogen in Si is an impurity that can adopt either positive, neutral, or negative charge states, depending on the Fermi level of the sample (here referred with respect to the valence band top energy  $E_v$ ). We define a chemical potential for electrons as  $\mu_e = E_v + E_F$ , where value of  $E_v$  is assumed to be constant and set to the highest occupied Kohn–Sham state of a 512-atom bulk calculation at  $\mathbf{k} = \Gamma$ . Hence, the free energy reference of Equation (1) is

$$F^{(0)} = \sum_i n_i \mu_i^{(0)} + n_e \mu_e = \sum_i n_i \mu_i^{(0)} - q(E_v + E_F) \quad (9)$$

where  $E_F$  is set *a priori* within the range  $0 \leq E_F \leq E_g$ , and  $n_e = -q$  is the number of extra electrons trapped at the defect with respect to the neutral charge state ( $q = 0$ ).

### 2.3. Activation Barriers and Rates

Within the statistical formulation of Vineyards's transition state theory,<sup>[71–73]</sup> the rate of a thermally activated process involving atomic motion is given by

$$\nu = \frac{k_B T}{h} \frac{Z^\ddagger}{Z} \quad (10)$$

where  $Z^\ddagger$  and  $Z$  are partition functions for the transition state and the initial state, respectively. Again, neglecting electronic excitations, assuming the harmonic approximation and a dilute regime (no interactions between defects and negligible impact on the Fermi level), we arrive at the following Arrhenius rate expression

$$\nu = \nu_0 \exp\left(-\frac{\Delta E_a}{k_B T}\right) \quad (11)$$

with the activation energy  $\Delta E_a = (E_{\text{elec}}^\ddagger + E_{\text{ZP}}^\ddagger) - (E_{\text{elec}} + E_{\text{ZP}})$  being obtained from a NEB calculation and the vibrational frequencies found as described in Section 2.1. The attempt frequency is given by

$$\nu_0 = \frac{Z_{\text{rot}}^\ddagger \prod_{i=1}^{3N-3} \nu_i}{Z_{\text{rot}} \prod_{i=1}^{3N-4} \nu_i} \quad (12)$$

which accounts for differences in rotational and vibrational degrees of freedom in the initial and transition states. For the

migration of  $H_2$  molecules, we will consider both  $Z_{\text{rot}}^{\ddagger}=1$  and  $Z_{\text{rot}}^{\ddagger}=Z_{\text{rot}}$ , representing partition functions for static and dynamic (rigid rotor) molecules at the transition state, respectively. The second fraction on the right-hand side of Equation (12) accounts for the phonon partition functions from the initial (numerator) and transition (denominator) states, respectively, to the attempt frequency. It is noted that the transition state only contributes with  $3N - 4$  vibrational modes, thus excluding the unstable mode along the jump trajectory.

Atomistic modeling of diffusing impurities in a  $d$ -dimensional medium usually starts with Einstein's relation for the diffusivity  $D = \langle \Delta r^2(t) \rangle / 2d\Delta t$ , where  $\langle \Delta r^2(t) \rangle$  is the mean square impurity displacement extrapolated to an interval of time  $\Delta t \rightarrow \infty$ . If the impurity travels according to random-walk statistics in a 3D crystal, then we have

$$D = \frac{g_j l_j^2 \nu}{6} \quad (13)$$

where  $\nu$  is the average rate of independent jumps of length  $l_j$  which can be performed along  $g_j$  equivalent paths for each initial state. For instance, bond-centered H has a total of  $g_j = 6$  available paths to perform a jump to its neighboring BC sites. Combining Equation (13) and (11), we can write the diffusivity in the Arrhenius form

$$D = D_0 \exp\left(-\frac{\Delta E_a}{k_B T}\right); \quad D_0 = \frac{g_j l_j^2 \nu_0}{6} \quad (14)$$

It is noted that quantum tunneling is not addressed. Such effects are expected to be more relevant at low temperatures ( $T \lesssim 80$  K).<sup>[74]</sup>

### 3. Results

#### 3.1. Relative Stability of Hydrogen Monomers and Dimers at $T = 0$

We start by reporting the energetics of hydrogen defects at  $T = 0$ . In this case, Equation (1) boils down to  $\Delta F_f(T = 0) = \Delta E_f$ , essentially involving the computation of the electronic plus ionic and zero-point vibrational energies of a defective supercell, subtracted by atomic and electronic chemical potentials

$$\Delta E_f = E_{\text{elec}} + E_{\text{ZP}} - \sum_i n_i \mu_i^{(0)} + q(E_v + E_F) \quad (15)$$

with  $\mu_i^{(0)}$  equally accounting for electronic and zero-point motion of the reference elements. **Figure 3** shows the calculated  $\Delta E_f$  for several H monomers. We recall that the chemical potential of H was found from the energy of a molecule at the T site. For that reason, its formation energy is zero (with and without accounting for zero-point motion). The main features of the diagram are well known, including the negative- $U$  ordering of donor and acceptor levels.<sup>[15,17,75]</sup> Here, we simply improve the results of previous calculations by applying a nonlocal functional to the many-electron energy. In practice, the current results are free from the underestimated bandgap syndrome typical of local and

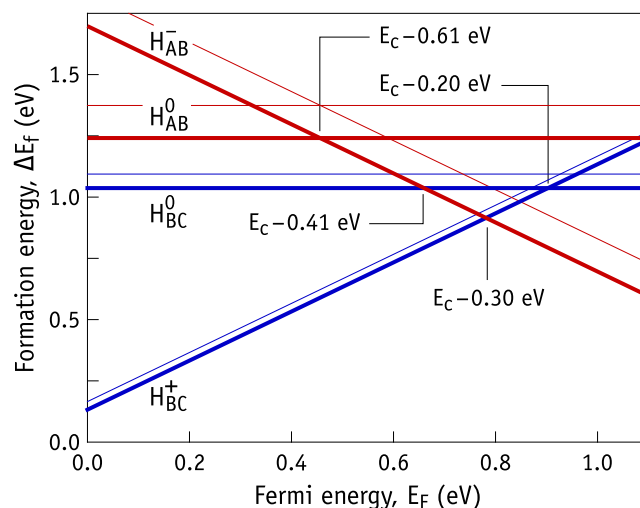


**Figure 3.** Energy of formation ( $\Delta E_f$ , thick lines) of hydrogen monomers in Si at  $T = 0$  K as a function of the Fermi level ( $E_F$ ). Only the electronic and zero-point vibrational energies are considered. For comparison, we also show the formation energy as obtained without the contribution of zero-point motion (thin lines). Calculated transition levels are also indicated.

semilocal approximations to the exchange–correlation interactions. It should be mentioned that the scissors correction applied to the local density results of Van de Walle et al. (Figure 11 of ref. [15]) turned out to provide a rather accurate picture. In the present case, the calculated bandgap, as found from the energy difference between the lowest unoccupied and highest occupied Kohn–Sham states, is  $E_g = 1.1$  eV.

Figure 3 shows formation energies that consider the electronic contributions only (thin lines), along with those that also account for the zero-point motion as well (thick lines). Blue and red lines represent  $\Delta E_f$  values for bond-centered and antibonding configurations, respectively.

In agreement with many previous reports,<sup>[15,17,19,75]</sup> positively charged H finds its ground state at the bond-centered site. Also like in other reports, the neutral state has two close energy structures, namely, the ground state at the BC site and a metastable state (0.20 eV above) with H located within the tetrahedral interstitial cage.

We find that the energy of tetrahedral interstitial  $H_T^0$  and  $H_T^-$  states are higher than  $H_{AB}^0$  and  $H_{AB}^-$  by, respectively, 0.15 and 0.04 eV. Although such small figures have little impact when estimating the location of the transition levels, it is important to refer that the  $H_T^0$  state in particular is definitely a local maximum of energy, whose height is comparable to the barrier for reorientation of  $H_{AB}^0$  within the T cage. Full HSE-level atomistic relaxations using smaller 64-Si-atom supercells confirm these findings within less than 10 meV. Another indication that  $H_T^0$  is not stable comes from a triply degenerate set of negative eigenvalues of the dynamical matrix for this structure, corresponding to an imaginary frequency of  $\nu = i520 \text{ cm}^{-1}$  (in addition to three translational modes). As for the negative state, the potential is very flat. Considering zero-point energy and zero-point motion effects, the energy difference between tetrahedral and

antibonding structures (40 meV) becomes irrelevant, and most probably  $H^-$  roams freely within the whole volume of the T cage even at  $T \sim 0$  K. The lower energy  $H_{AB}^-$  was the structure employed in the calculations presented below (unless specified otherwise). It is unclear why  $H_T$  is a maximum in the potential energy surface. The defect introduces a singlet state in the gap, and we can only suggest that the off-site location could be driven by a pseudo-Jahn–Teller effect.

Regarding the calculated charge state transition levels, we obtain a donor transition at  $E_c - 0.20$  eV involving the  $H_{BC}$  structure (blue lines in Figure 3). This is very close to the  $E_3'$  electron trap measured at  $E_c - 0.175$  eV.<sup>[11,76]</sup> An acceptor at  $E_c - 0.61$  eV ( $E_v + 0.49$  eV) was also found, but now involving the  $H_{AB}$  configuration (red lines in Figure 2). Considering that  $H_{BC}^0$  is the actual ground state for neutral H (lying 0.2 eV below  $H_{AB}^0$ ), the thermodynamic acceptor level is therefore at  $E_c - 0.41$  eV ( $E_v + 0.69$  eV), which combined with the donor transition leads to a negative- $U$  ( $-/+$ ) level at  $E_c - 0.30$  eV. Both the acceptor and negative- $U$  levels edge the ranges  $E_c - E(-/0) = 0.4 - 0.6$  eV and  $E_c - E(-/+ ) = 0.3 - 0.4$  eV, estimated by junction capacitance measurements.<sup>[23]</sup>

According to Van de Walle and Neugebauer,<sup>[77]</sup> a universal charge neutrality level (UCNL) that pins the ( $-/+$ ) transition of hydrogen was postulated at about  $-4.5$  eV with respect to vacuum. For the case of Si, this is located at  $E_c - 4.5$  eV +  $\chi = E_c - 0.4$  eV, where  $\chi = 4.1$  eV is the electron affinity of crystalline Si.<sup>[78]</sup> Importantly, if we allow for 1) some spread in the ( $-/+$ ) transition estimated by the UCNL method (due to for instance dielectric screening variance—a spread of about 0.4 eV was found after considering a range of semiconductors and insulators<sup>[77]</sup>), 2) for the uncertainty in the measurements ( $\approx 0.1$  eV), and 3) for the typical error bar of our calculations ( $\approx 0.1$  eV), we find an overlap and consistency among all three methods.

Figure 2 shows that zero-point motion effects can have a sizable impact regarding the location of the levels. Bond-centered hydrogen defects have a zero-point vibrational contribution  $\Delta E_{ZP} = E_{ZP} - E_{ZP}^{(0)} \approx 0.1$  eV, where  $E_{ZP}^{(0)}$  is the zero-point energy of the reference elements (bulk Si and molecular hydrogen in Si). This figure is about twice as much found for antibonding monomers (see Table 1). The formation energies incorporating the zero-point motion (thick lines in Figure 2) are below the electronic formation energies (thin lines) because their respective references differ by  $\Delta E_{ZP}(H_{2T})/2 = 0.18$  eV, which is the zero-point motion contribution to the H chemical potential. The results are qualitatively in line with those obtained by Karazhanov and co-workers,<sup>[20]</sup> but quantitatively different. We find deviations of just above  $\approx 0.1$  eV in the location of the electronic levels after considering zero-point energies, perhaps because we considered the vibrational modes of all atoms in the supercells. In Karazhanov et al.,<sup>[20]</sup> only a few atoms around the defects were considered for constructing the dynamical matrix.

As for the relative stability of hydrogen dimers we find that  $H_2^*$  is metastable by 0.19 eV with respect to  $H_{2T}$ . This result includes the zero-point energy difference (0.01 eV higher in  $H_2^*$ ) and it is in line with previous reports as well (see Estreicher et al.<sup>[6]</sup> and references therein). Based on such a small energy difference, it is

difficult to understand the exclusive formation of molecular  $H_2$  in samples quenched from high temperatures.

We could not find any additional dimer whose stability was comparable to that of  $H_{2T}$  and  $H_2^*$ . The third most favorable geometry for a pair of hydrogen atoms in silicon was made of two antibonding Si– $H_{AB}$  units sitting on opposite sides of a Si–Si broken bond. This structure, previously referred to as  $H_2^{**}$ ,<sup>[79]</sup> was less stable than  $H_{2T}$  by 1.1 eV. Hence, our results cannot explain the existence of a third dimer ( $H_{2B}$ ) as proposed in the study by Voronkov and Falster,<sup>[32]</sup> unless its formation involves an extrinsic impurity that provides a stabilizing effect. However, this possibility presents difficulties regarding an explanation for the fast diffusing nature of  $H_{2B}$ , whose activation energy was estimated to be as low as 0.53 eV.<sup>[32]</sup>

### 3.2. Migration and Reconfiguration

Figure 4 shows a CCD for atomic hydrogen in p-type Si, constructed from the formation energies at  $T = 0$  and calculated migration/transformation barriers also at  $T = 0$ . The transition states were found using a 13-image-NEB method (see Section 2.1) and account for the zero-point energy of  $3N - 4$  vibrational modes. The three charge states, namely, positive (blue line), neutral (green line), and negative (red line), are offset in the energy scale by hole emission energies  $E(0/+) - E_v = 0.90$  eV and  $E(-/0) - E_v = 0.69$  eV.

As expected, the migration mechanism of  $H_{BC}^+$  was found along the shortest path passing close to the C-point. The process is depicted in the structure of Figure 4a. The transition state lies 0.42 eV above the ground state, underestimating the value measured at low temperatures merely by 0.01 eV<sup>[8]</sup> and underestimating the high-temperature data by 0.06 eV.<sup>[24]</sup>

An interesting property of the antibonding configuration of  $H_{AB}^-$  is that the migration mechanism is not along the  $\langle 111 \rangle$  crystalline directions (passing by the hexagonal site) as previously assumed for  $H_T^-$ . Instead, the hydrogen moves through the hexagonal channels along  $\langle 110 \rangle$  directions as depicted in Figure 4c. Still the transition state is very close to the hexagonal site and the estimated barrier is  $\Delta E_a = 0.47$  eV, i.e., 0.05 eV higher than that for the migration of  $H_{BC}^+$ . Consistently with previous theoretical estimates, the barrier is much lower than the 0.7 eV activation energy obtained from the kinetic studies of the release/retrapping of H by dopants upon injection of minority carriers.<sup>[42]</sup>

Now we look at the neutral state. Hole emission from neutral hydrogen must be preceded by a reconfiguration to the  $H_{AB}^0$  metastable state. This process is represented by the arrow with label “1” in the structure of Figure 4b. The potential energy close to  $H_{AB}^0$  is represented in the CCD as a dashed green line with a minimum 0.2 eV above  $H_{BC}^0$ . The calculated barrier for the  $H_{BC}^0 \rightarrow H_{AB}^0$  reconfiguration is  $\Delta E_a = 0.36$  eV. However, as the barrier for returning to the  $H_{BC}^0$  ground state is only  $\Delta E_a = 0.16$  eV, hole emission from the metastable state  $H_{AB}^0 \rightarrow H_{AB}^- + h^+$  (with emission energy  $\Delta E = 0.49$  eV) is highly unlikely. This makes the direct observation of the ( $-/0$ ) transition an extremely difficult task to be performed by charge-countable techniques such as DLTS.

**Table 1.** Calculated and measured properties of hydrogen monomers and dimers in silicon. Quantities reported in the second column include: configurational degeneracy per unit cell ( $g$ ), bond lengths ( $d$ ), zero-phonon energies ( $\Delta E_{ZP}$ ), activation energies ( $\Delta E_a$ ), attempt frequencies ( $\nu_0$ ), jumping degeneracy ( $g_j$ ), jump distance ( $l_j$ ), reconfiguration and carrier emission energies ( $\Delta E$  is positive/negative for endothermic/exothermic processes), diffusivity prefactors ( $D_0$ ), and LVM frequencies. Several measured quantities and references can be found in the third column.

	Calculated	Measured
$H_{BC}^+$	$g = 4$ , $d_{Si-H} = 1.592 \text{ \AA}$ , $\Delta E_{ZP} = 0.14 \text{ eV}$	–
$H_{BC}^+ \xrightarrow{\text{migration}} H_{BC}^+$	$\Delta E_a = 0.42 \text{ eV}$ , $\nu_0 = 1.4 \text{ THz}$ , $g_j = 6$ , $l_j = 1.92 \text{ \AA}$	$\nu_0 = 2.3 \text{ THz}$ , $\Delta E_a = 0.43 - 0.44 \text{ eV}$ [8,11]
$H_{BC}^+ \rightarrow H_{BC}^0 + h^+$	$\Delta E = 0.90 \text{ eV}$	–
LVM frequencies	$2112 \text{ cm}^{-1}$	$1998 \text{ cm}^{-1}$ [80]
$H_{BC}^0$	$g = 4$ , $d_{Si-H} = 1.614 \text{ \AA}$ , $\Delta E_{ZP} = 0.12 \text{ eV}$	–
$H_{BC}^0 \rightarrow H_{BC}^+ + e^+$	$\Delta E = 0.20 \text{ eV}$	$\Delta E = 0.175 - 0.2 \text{ eV}$ [11,76]
$H_{BC}^0 \xrightarrow{\text{migration}} H_{BC}^0$	$\Delta E_a = 0.36 \text{ eV}$ , $\nu_0 = 9.4 \text{ THz}$ , $g_j = 6$ , $l_j = 1.92 \text{ \AA}$	–
$H_{BC}^0 \xrightarrow{\text{reconf.}} H_{AB}^0$	$\Delta E = 0.20 \text{ eV}$ , $\Delta E_a = 0.36 \text{ eV}$ , $\nu_0 = 9.4 \text{ THz}$	$\Delta E_a = 0.293 \text{ eV}$ , $\nu_0 = 3 \text{ THz}$ [11]
$2H_{BC}^0 \rightarrow H_{BC}^+ + H_{AB}^-$	$\Delta E = -0.21 \text{ eV}$	–
LVM frequencies	$1998 \text{ cm}^{-1}$	–
$H_{AB}^0$	$g = 8$ , $d_{Si-H} = 1.675 \text{ \AA}$ , $\Delta E_{ZP} = 0.04 \text{ eV}$	–
$H_{AB}^0 \rightarrow H_{AB}^- + h^+$	$\Delta E = 0.49 \text{ eV}$	–
$H_{AB}^0 \xrightarrow{\text{migration}} H_{AB}^0$	$\Delta E_a = 0.04 \text{ eV}$ , $\nu_0 = 5.4 \text{ THz}$ , $g_j = 6$ , $l_j = 2.01 \text{ \AA}$	$\Delta E_a < 0.1 \text{ eV}$ [23]
$H_{AB}^0 \xrightarrow{\text{reconf.}} H_{BC}^0$	$\Delta E = -0.20 \text{ eV}$ , $\Delta E_a = 0.16 \text{ eV}$ , $\nu_0 = 2.1 \text{ THz}$	$\Delta E_a \approx 0.2 \text{ eV}$ [11]
LVM frequencies	$1114 \text{ cm}^{-1}$	–
$H_{AB}^-$	$g = 8$ , $d_{Si-H} = 1.771 \text{ \AA}$ , $\Delta E_{ZP} = 0.07 \text{ eV}$	–
$H_{AB}^- \rightarrow H_{AB}^0 + e^-$	$\Delta E = 0.61 \text{ eV}$	$\Delta E = 0.56 \text{ eV}$ [10]
$H_{AB}^- \rightarrow H_{BC}^0 + e^-$	$\Delta E = 0.41 \text{ eV}$	$\Delta E = 0.4 - 0.6 \text{ eV}$ [23]
$H_{AB}^- \xrightarrow{\text{migration}} H_{AB}^-$	$\Delta E_a = 0.47 \text{ eV}$ , $\nu_0 = 9.6 \text{ THz}$ , $g_j = 6$ , $l_j = 2.03 \text{ \AA}$	$\Delta E_a \lesssim 0.7 \text{ eV}$ [42]
LVM frequencies	$(920, 695) \text{ cm}^{-1}$	–
$H_2^*$	$g = 8$ , $d_{Si-H(BC)} = 1.512 \text{ \AA}$ , $d_{Si-H(AB)} = 1.548 \text{ \AA}$ , $\Delta E_{ZP} = 0.36 \text{ eV}$	–
$H_2^* \xrightarrow{\text{reconf.}} H_{2T}$	$\Delta E = -0.19 \text{ eV}$ , $\Delta E_a = 1.43 \text{ eV}$	–
LVM frequencies	$(2078, 1805, 776, 775) \text{ cm}^{-1}$	$(2062, 1838) \text{ cm}^{-1}$ [27]
$H_{2T}$ molecule	$g = 2$ , $d_{H-H} = 0.778 \text{ \AA}$ , $\Delta E_{ZP} = 0.35 \text{ eV}$	–
$H_{2T} \xrightarrow{\text{migration}} H_{2T}$	$\Delta E_a = 0.82 \text{ eV}$ , $D_0 = 3.4 \times 10^{-4} \text{ cm}^2 \text{ s}^{-1}$ , $g_j = 4$ , $l_j = 2.35 \text{ \AA}$	$D_0 = 2.6 \times 10^{-4} \text{ cm}^2 \text{ s}^{-1}$ , $\Delta E_a = 0.78 \text{ eV}$ [35]
$H_{2T} \xrightarrow{\text{reconf.}} H_2^*$	$\Delta E = 0.19 \text{ eV}$ , $\Delta E_a = 1.62 \text{ eV}$ , $\nu_0 = 5.4 \text{ THz}$	–
LVM frequencies	$3687 \text{ cm}^{-1}$	$3618 \text{ cm}^{-1}$ [33,34]

In line with previous results,<sup>[6]</sup> the calculated barrier for the hopping of a neutral H atom between BC sites is considerably higher than that between AB sites. Small differences were found though. We find that the minimum energy path between two neighboring  $H_{BC}^0$  states is along the  $H_{AB}^0$  configuration, corresponding to the already mentioned mechanism shown by the arrow “1” in Figure 4b, with a barrier of  $\Delta E_a = 0.36 \text{ eV}$ . Jumps in the direction of the C-point (cf., structure of Figure 4a) correspond to a barrier  $\Delta E_a = 0.44 \text{ eV}$  high. On the other hand, jumps between  $H_{AB}^0$  states along the hexagonal channel in the  $\langle 110 \rangle$  direction (arrow “2” in Figure 3b) involve surmounting a minute barrier of only  $0.04 \text{ eV}$  (including zero-point energy contributions).

Of course, depending on the temperature, doping type and concentration, and the presence of photogenerated or injected minority carriers, the hydrogen atom can reside temporarily in the  $H_{AB}^0$  state and perform several jumps along such a flat potential landscape before returning to the  $H_{BC}^0$  ground state. Essentially, the migration of neutral H could be described by a thermally activated  $H_{BC}^0 \rightarrow H_{AB}^0$  jump ( $\Delta E_a = 0.36 \text{ eV}$  followed by the reverse process) with an effectively long traveling distance that depends on the lifetime of the metastable  $H_{AB}^0$  state. This effect is qualitatively addressed in Section 3.4.

The lowest energy configuration of the hydrogen molecule in Si has the H—H bond along  $\langle 111 \rangle$  directions. In agreement with previous studies, we found that  $H_{2T}$  can rotate almost freely in



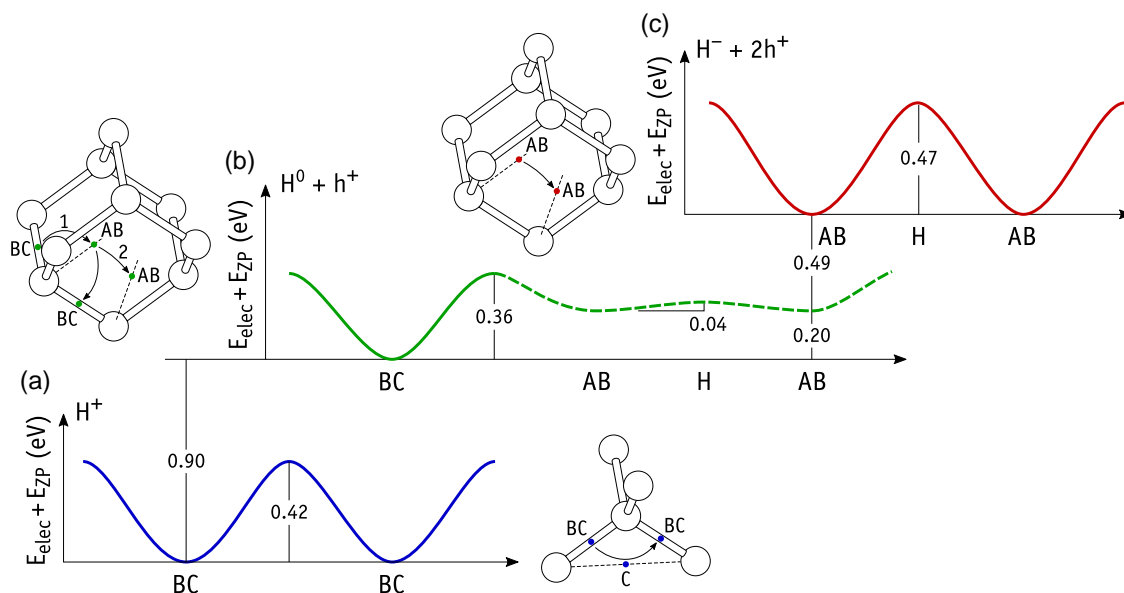


**Figure 4.** Calculated CCD for atomic hydrogen in silicon. All minima and barriers indicated account for electronic (plus ionic) and zero-point vibrational energies. CCDs for charge states a) plus, b) neutral, and c) negative are offset in the energy scale by  $E(0/+)-E_v = 0.90$  eV and  $E(-/0)-E_v = 0.69$  eV eV, corresponding to the energy for hole emission from  $H_{BC}^+$  and  $H_{BC}^0$  ground states to the valence band top.

the T site.<sup>[28,68]</sup> The energy of other molecular alignments differed by less than 5 meV.

We also investigated the reconfiguration and migration of hydrogen dimers. Regarding the transformation  $H_{2T} \rightarrow H_2^*$ , we found that the most favorable mechanism involves the collision of  $H_{2T}$  molecules with Si—Si bonds. Taking, for instance, a molecule at the central T site of Figure 1, the collision with one of the 12 nearest BC sites (e.g., the one indicated with a blue dot) results in the breaking of the H—H bond and the formation of a metastable  $(H_{BC}-H_{AB})^*$  complex. This is expected to be the rate-limiting step for the breaking of  $H_{2T}$  without the assistance of defects. In this complex, the Si— $H_{BC}$ —Si unit is slightly bent toward the C site, while the  $H_{AB}$  atom is very close to the original T site of the molecule. The reaction  $H_{2T} \rightarrow (H_{BC}-H_{AB})^*$  has an activation energy of  $\Delta E_a = 1.62$  eV and the resulting metastable complex is  $\Delta E = 1.14$  eV higher in energy than  $H_{2T}$ . Further displacement of the  $H_{BC}$  unit to finally form  $H_2^*$  involves surmounting a barrier of only 0.40 eV, i.e., the second transition state is 1.54 eV above the initial  $H_{2T}$  state.

Instead of breaking, the  $H_{2T}$  molecule can migrate across the lattice. The migration of  $H_{2T}$  in Si is commonly described as involving the motion of the molecules between T sites through H sites with their H—H bonds parallel to the direction of motion (perpendicular to the hexagonal rings). Our results suggest that this is not the best picture. We found that the energy of the molecule at the H site depends very little on its crystalline orientation. In fact, the transition state along the minimum energy path is the one with the H—H bond perpendicular to the direction of motion. Considering zero-point motion effects, the barrier is  $\Delta E_a = 0.82$  eV high, and this is only 0.02 eV lower than if we considered a transition state with the H—H bond along the  $\langle 111 \rangle$  direction of motion. This figure is very close to the activation energy  $\Delta E_a = 0.78$  eV for the capture kinetics

of migrating  $H_2$  molecules by interstitial oxygen impurities.<sup>[35]</sup> In Section 3.4, we will argue that the molecules should be treated as nearly free rotors all along the migration path, including at the transition state.

The above results demonstrate that the barrier for breaking the molecules is almost twice that for the migration. Assuming a typical pre-exponential factor of  $\nu_0 \approx 10^{12} \text{ s}^{-1}$  for a thermally activated process, a dissociation rate of  $\nu \approx 1 \text{ s}^{-1}$  for the breaking of the molecules is reached when the temperature is nearly 400 °C. It appears that the lifetime of  $H_{2T}$  significantly exceeds that of  $H_2^*$  (according to the experimental results,  $H_2^*$  is not thermally stable above 200 °C<sup>[27]</sup>). Therefore, it can be suggested that during quenching from high temperatures, there is a wide temperature window of  $\approx 200 - 400$  °C where the molecule can form, migrate, and react with defects and impurities, avoiding formation of  $H_2^*$ .

### 3.3. Stability of Hydrogen Species at Finite Temperatures

We start the reporting of the finite temperature results with a comparison of the relative stability of  $H_{2T}$  and  $H_2^*$ . The results are summarized in Figure 4, where we show the total free energy of both defects calculated according to Equation (2) in the temperature range  $T = 0 - 800$  K on the left, and their difference,  $\Delta F_{\text{dimers}} = F(H_2^*) - F(H_{2T})$ , as a thick solid line on the right. The thin solid lines in Figure 5b represent partial contributions from the electronic plus ionic potential (elec), vibrational modes calculated in 64 Si atom cells (vib), rotational states of  $H_{2T}$  (rot), and configurational entropy (conf). For this specific case, the configurational entropy accounts for the different number of orientations of each species and does not depend on the concentration of hydrogen in the silicon.

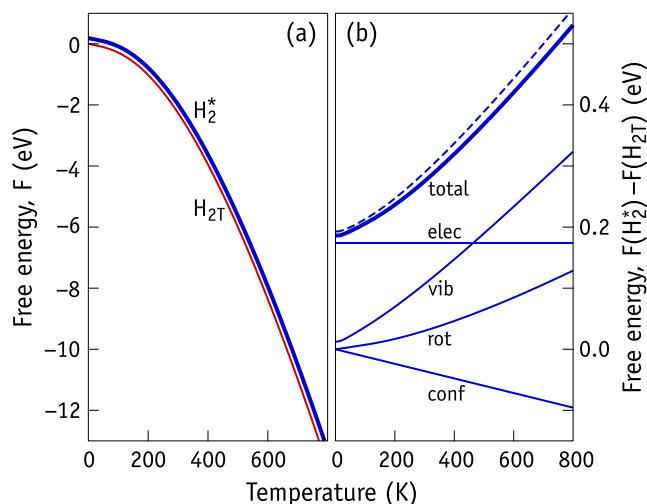


**Figure 5.** a) Free energy of  $H_2^*$  (blue line) and  $H_{2T}$  (red line) in the temperature range  $T = 0 - 800$  K. b) Difference between free energies of  $H_2^*$  and  $H_{2T}$  in silicon,  $F(H_2^*) - F(H_{2T})$ , represented as a thick solid line. Partial contributions from the electronic plus ionic potential (elec), vibrational modes calculated in 64 Si atom cells (vib), rotational states of  $H_{2T}$  (rot), and configurational entropy (conf) are also shown as thin solid lines. The dashed curve represents the same quantity obtained using a larger supercell with 216 atoms for the evaluation of the vibrational free energy.

The dashed line in Figure 5b represents the formation energy difference between  $H_2^*$  and  $H_{2T}$ , with the vibrational free energy obtained from larger 216-Si-atom cells (645 normal modes of vibration). Clearly, the number of phonons represented by the smaller cells is sufficient for the present purpose.

At a glance, Figure 5a does not provide us with much information, apart from the fact that no matter the temperature  $H_2^*$  is less stable than  $H_{2T}$ . More interesting conclusions can be drawn from analysis of  $\Delta F_{\text{dimers}}$ , as shown in Figure 5b. In this figure it is clear that  $H_2^*$  becomes less favorable with increasing the temperature, or alternatively, the molecule becomes progressively more stable. These findings are in line with previous results by Estreicher and co-workers.<sup>[28]</sup>

The electronic component of  $\Delta F_{\text{dimers}}$ , evaluated from 512 atom cells plus defects, gives  $\Delta E_{\text{elec}} = 0.17$  eV. Zero-point motion increases  $\Delta F_{\text{dimers}}(T = 0)$  to  $\Delta E = 0.19$  eV. At finite temperatures, the dominant contribution to  $\Delta F_{\text{dimers}}$  comes from the vibrational degrees of freedom. The effect of molecular rotation cannot be neglected and nearly compensates for the configurational entropy difference between both defects (the number of possible locations/orientations per unit cell is  $g = 8$  and 2 for  $H_2^*$  and  $H_{2T}$ , respectively). At  $T = 500$  K, which is approximately the annealing temperature of  $H_2^*$ , the free energy difference increases to  $\Delta F_{\text{dimers}}(T = 500 \text{ K}) = 0.37$  eV. At  $T \approx 700$  K, which is our estimated temperature for the breaking of the molecules due to collisions against the Si—Si bonds,  $\Delta F_{\text{dimers}}$  raises to almost 0.5 eV. Again, this effect is consistent with the observed formation of molecules (and not  $H_2^*$  dimers) when the Si is quenched after heat treatments at temperatures higher 700 °C in the presence of a hydrogen source.

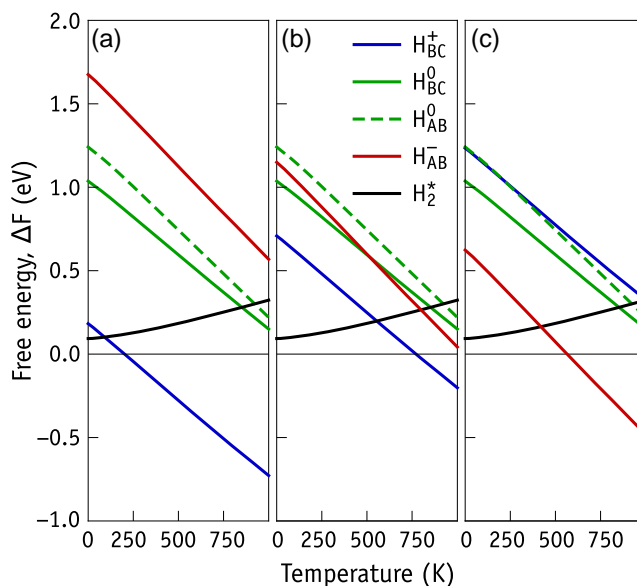


**Figure 6.** Temperature dependence of the free energy of formation per hydrogen atom for several H-defects in Si with respect to the same quantity for molecular  $H_2$  in Si. a) For the Fermi level at the valence band top, b) for the Fermi level at midgap, and c) for the Fermi level at the conduction band bottom. The configurational entropy was evaluated considering a concentration of H monomers and dimers of  $2 \times 10^{14}$  and  $1 \times 10^{14} \text{ cm}^{-3}$ , respectively.

Figure 6 depicts the free energy change per H atom,  $\Delta F = F(X_n)/n - F(H_{2T})/2$ , of several H defects  $X = \{H_2^*, H_{BC}^+, H_{BC}^0, H_{AB}^0, H_{AB}^-\}$  with  $n = \{1, 2\}$  being the number of H elements in each defect. The zero energy refers to a sample of bulk silicon with a concentration  $1 \times 10^{14} \text{ cm}^{-3}$  of  $H_{2T}$  molecules at a specific temperature  $T$ . The calculations were carried out in the temperature range  $T = 0 - 1000$  K. For the calculation of the configurational entropy, concentrations of  $2 \times 10^{14}$  and  $1 \times 10^{14} \text{ cm}^{-3}$  were assumed for H monomers and dimers, respectively. Three distinct situations are considered in the figure, namely, when the Fermi energy is located a) at the top of the valence band, b) at midgap, and c) at the bottom of the conduction band. Figure 6b is the one that intends to reproduce the intrinsic conditions attained at high temperatures.

Regarding the  $H_2^*$  (black line), the plot essentially reproduces the results of Figure 5b. As for the monomers, their free energy with respect to that of  $H_{2T}$  decreases with  $T$ . This is mostly a configurational entropy effect which notably makes  $H_{BC}^+$  and  $H_{AB}^-$  more stable than  $H_{2T}$  in p-type and n-type Si above  $T \approx 250$  and 550 K, respectively (cf., Figure 6a,c). However, at these temperatures and above, any existing molecule that was not trapped by other impurities or defects must overcome the 1.6 eV dissociation barrier before the hydrogen atoms can capture holes or electrons to end up as 2  $H_{BC}^+$  or 2  $H_{AB}^-$ , respectively. Of course,  $H_{BC}^+$  and  $H_{AB}^-$  are fast diffusing species and anneal out well below room temperature.

Under intrinsic conditions and at temperatures high enough to release the hydrogen from traps,  $H_{BC}^+$  becomes the most

favorable hydrogen defect above  $T \approx 750$  K ( $T \approx 480$  °C). This provides an estimate for the temperature below which  $H_{2T}$  formation becomes thermodynamically favorable with respect to the dissociated state.

The rate of change of the free energies with the temperature is also different among the H species. The free energy of bond-centered defects, shown in Figure 6 as solid blue and solid green lines, has a similar (almost parallel) change with  $T$ , dominated by the configurational entropy. The vibrational and rotational (from the molecule reference) free energy contributions have opposite signs (negative and positive, respectively) and almost cancel. The decreasing rate of  $\Delta F$  for the antibonding configurations is slightly faster, especially for the negatively charged  $H_{AB}^-$  state (solid red line). We will further investigate this effect in the future. Presently, we can only suggest that the antibonding configurations soften the neighboring Si—Si bonds, leading to a compression of the spacing between the excited vibrational states of crystalline modes localized around the defect, to an increasingly number of accessible states at finite temperatures, and, therefore, to an increase of the vibrational entropy,  $-TS_{vib}$ .

Interestingly, because of the above effect, at  $T \gtrsim 500$  K under intrinsic conditions  $H_{AB}^-$  becomes the second most stable monomer after  $H_{BC}^+$ . This result allows us to propose the following interpretation of the effective formation of molecular hydrogen during the cooling of hydrogenated samples from high temperatures ( $T \gtrsim 700$  °C): 1) above  $T \approx 700$  K the molecules are not stable and free hydrogen may only be detected transiently in the atomic form, mostly as  $H_{BC}^+$ , but also as a small fraction of  $H_{AB}^-$ ; 2) below  $T \approx 700$  K, the interaction between  $H_{BC}^+$  and  $H_{AB}^-$  leads to the formation of stable  $H_{2T}$  molecules; 3) with further cooling,  $H_{AB}^-$  is further consumed by  $H_{BC}^+$ , and formation of molecules occurs as long as the temperature remains above  $T \approx 500$  K, below which the fraction of  $H_{AB}^-$  becomes negligible in comparison to other states, and  $H_{2T}$  formation stops.

We will also argue in the next section that the formation of  $H_{AB}^-$  at high temperatures has implications to the diffusivity of hydrogen.

### 3.4. Diffusivity of Hydrogen in Silicon

In this section, we report our results pertaining to the diffusivity of hydrogen species, including the effects of temperature. Migration barriers were already reported in Section 3.2, and now we look at the attempt frequencies (Equation (12)), temperature-dependent jump rates (Equation (11)), and diffusivities (Equation (14)).

The calculations were carried out considering the Fermi level pinned to midgap. This impacts free energies of formation and the mix of H monomers participating in atomic hydrogen transport. On the other hand, given that  $H_{2T}$  is electrically inactive, results pertaining to its diffusivity are independent of the doping type.

Below we discuss the diffusivity of H monomers in the context of the high-temperature measurements of VWW ( $T \approx 1400$  K) and the low-temperature measurements of GN ( $T \approx 130$  K). At high temperatures, dopants are expected to play a negligible effect on H diffusivity and the results are valid for any doping type. At low temperatures, the results represent the diffusivity

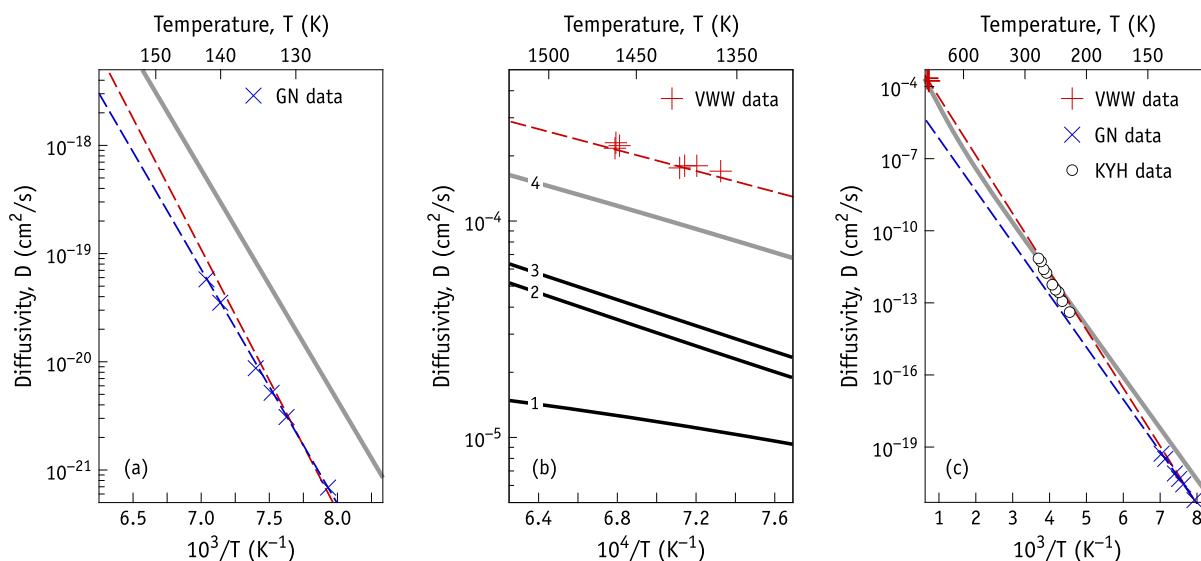
of  $H^+$  alone (or  $H^+$  elementary jumps as monitored in the GN experiments). They are applicable to intrinsic and p-type Si, and do not account for eventual trapping effects by dopants and impurities. Molecular diffusivity can be neglected at such low temperatures.

Figure 7 shows three Arrhenius plots of the diffusivity of atomic hydrogen versus temperature in different temperature ranges. In Figure 7a, the low-temperature measurements by Nevinnyi and Gorelkinsky are represented by crosses (GN data) and the best Arrhenius fit to the data gives  $\nu_0 = 0.3$  THz and  $\Delta E_a = 0.43$  eV<sup>[8,17]</sup> (blue dashed line). These figures pertain to the jump of  $H_{BC}^+$  between bond-centered sites because the stress alignment of the hydrogen defects in these experiments was carried out in darkness, where only anisotropic  $H_{BC}^+$  could form. Considering the  $3N - 3 = 189$  phonon frequencies obtained for the ground state of  $H_{BC}^+$ , as well as the analogous  $3N - 4 = 188$  phonon frequencies for the transition state between two neighboring BC sites, we arrive at a frequency of attempt  $\nu_0 = 1.4$  THz, nearly a factor of five higher than the figure extracted from the measurements. Considering that during migration each proton can perform  $g_j = 6$  equivalent jumps of length  $l_j = 1.92$  Å, we arrive at a calculated diffusivity  $D(T) = (5.3 \times 10^{-4} \text{ cm}^2 \text{ s}^{-1}) \exp(-0.42 \text{ eV}/k_B T)$ . This result is shown in Figure 7a as a solid gray line, above the experimental diffusivity. Considering the error bars typically involved in the calculation of  $\nu_0$  (easily up to a factor of 5), we take the match between the calculations and the measurements as acceptable.

Comparing the measured low- $T$  diffusivity with the measurements extrapolated from the VWW data (red dashed line in Figure 7a), we find a surprising agreement. Of course, the potential errors in such extreme extrapolation must be considered, particularly as the VWW data have noticeable scatter and were measured only over a relatively narrow range of temperatures. Yet if we insist in pursuing such an exercise, we find that at high temperatures the diffusivity is enhanced by several decades (Figure 7c). The obvious question would be: What is the root cause for the bowing in the hydrogen diffusivity in Si?

Considering that the path-integral Monte Carlo calculations by Herrero<sup>[74]</sup> indicate that tunneling motion of bond-centered H in silicon only takes place below  $T \lesssim 80$  K, the low- $T$  GN data of Figure 6a are expected to be well described by classical transition-state theory. It is therefore more likely that any eventual acceleration in the diffusivity should occur at high temperatures. The high- $T$  data are shown in Figures 7b,c as “plus” symbols. The best fit to the data, shown as a red dashed line, gives  $D = (9.4 \times 10^{-3} \text{ cm}^2 \text{ s}^{-1}) \exp(-0.48 \pm 0.05 \text{ eV}/k_B T)$ , and it is above the extrapolated low-temperature diffusivity (blue dashed line) by a factor of  $\approx 8$ .

It was proposed in the study by Voronkov and Falster<sup>[41]</sup> that a fast diffusing neutral hydrogen, although present in small quantities even at  $T \approx 1000$  °C, could lead to the observed enhancement of the diffusivity. Based on the calculated free energies of all four studied hydrogen monomers ( $H_{BC}^+$ ,  $H_{AB}^-$ ,  $H_{BC}^0$ , and  $H_{AB}^0$ ), we estimated their equilibrium fractional concentrations as a function of temperature as  $c_m = p_m/Z$ , with  $p_m = \exp(-F_m/k_B T)$ ,  $Z = \sum_m p_m$  and  $F_m$  is the temperature dependent free energy of species  $m$  (which is an index that runs



**Figure 7.** Calculated diffusivity of atomic hydrogen in silicon (solid lines) along with measured data (symbols and dashed lines). a) Low-temperature region with the GN data,<sup>[8]</sup> extrapolated VWW diffusivity (dashed red line), and calculated diffusivity (gray solid line). b) High-temperature region with the VWW data<sup>[24]</sup> along with the calculations showing the cumulative effect of considering 1)  $H_{BC}^+$ , 2)  $H_{AB}^-$ , 3)  $H_{BC}^0$ , and 4)  $H_{AB}^0$  species to the weighted total diffusivity (solid gray line). c) Extrapolation of the diffusivities from the high-temperature and low-temperature data using Arrhenius relations (dashed lines). The intermediate temperature data of KYH<sup>[25]</sup> are also shown.

over all monomers). For the calculation of the free energies, the Fermi level was assumed to be locked at mid-gap, which is adequate to describe the high temperature conditions. An effective diffusivity  $D_{\text{eff}} = \sum_m c_m D_m$  was evaluated from calculated attempt frequencies for jumping of all four species ( $\nu_0$ ), activation energies for migration ( $\Delta E_a$ ), number of equivalent jumps ( $g_j$ ), and respective lengths ( $l_j$ ). All these data are summarized in Table 1.

Figure 7b shows the cumulative effect of progressively adding the contribution of migrating species to the total diffusivity. The line with label 1 represents the diffusivity obtained when only  $H_{BC}^+$  is considered. This is an extrapolation of the Arrhenius relation represented by the thick gray line in Figure 7a. At 1500 K the calculated  $H_{BC}^+$  diffusivity it is only  $\approx 2.5$  times higher than the value extrapolated from the low- $T$  measurements (blue dashed line), but about 20 times lower than the high- $T$  data. At the same temperature, the diffusivity is enhanced by  $\approx 3$  times if in addition to  $H_{BC}^+$  we consider the presence of negatively charged  $H_{AB}^-$  species (line 2). Under these conditions,  $H_{AB}^-$  is the second most stable monomer (see Figure 6b) with a free energy of 0.12 eV above  $H_{BC}^+$  and a relative population  $p \approx 1/4$ . Although the calculated activation energy for migration ( $\Delta E_a = 0.47$  eV) is slightly higher than that of the proton, the pre-exponential factor is also larger, almost by a factor of 7. A large pre-exponential factor indicates a saddle point that is “wide” in the configurational space and “highly probable to surmount,” as opposed to a small frequency of attempt which is typical of “narrow” transition states which are “less probable to surmount.”

If we continue with adding the remaining monomers to the diffusing mix, we find that the most stable bond-centered neutral hydrogen leads to a small enhancement (line 3), mostly due to its minute concentration. However, the free energy of  $H_{AB}^0$  decreases faster with temperature than that  $H_{BC}^0$  (see Figure 6b),

and at  $T = 1500$  K (intrinsic Si) both states essentially become degenerate, with a free energy about 0.34 eV above  $H_{BC}^+$ . The result of the participation of  $H_{AB}^-$  and especially of fast diffusing  $H_{AB}^0$  (in addition to  $H_{BC}^+$ ) in the diffusing mix is an enhancement of the diffusivity by a factor of ten. Of course, there are large errors, especially because at such high temperatures the harmonic approximation is no longer applicable. However, the effect is qualitatively visible as a bowing in the calculated diffusivity at high temperatures in Figure 7c.

We now turn our attention to the diffusivity of the hydrogen molecule in Si. We saw in Section 3.2 that the  $H_{2T}$  molecule has a relatively low migration barrier ( $\Delta E_a = 0.82$  eV) when compared to the barrier for conversion to  $H_2^*$  ( $\Delta E_a = 1.62$  eV). This implies that the molecule anneals via migration and dissociation is most likely to occur with the action of a defect which could react with the molecule. We also found that the variation of the potential energy with rotation of the molecule is a few meV in both stable (T site) and transition (H site) states, suggesting that  $H_{2T}$  migrates as a free rotor and not a static dimer aligned along the hexagonal ring.

We calculated the attempt frequency for molecular jumping between T sites (Equation (12)), assuming either a static ( $Z_{\text{rot}}^{\ddagger} = 1$ ) or a dynamic transition state ( $Z_{\text{rot}}^{\ddagger}$  given by Equation (8)). In the first case, the attempt frequency is reduced by a factor  $1/Z_{\text{rot}}$ , which accounts for the narrowing of the saddle point due to the absence of rotational freedom on that state. The hindering effect is further enhanced with raising the temperature. At  $T = 0$  K the reducing factor is  $1/Z_{\text{rot}} = 1$  and the attempt frequency  $\nu_0 = 0.93$  THz. However, the latter decreases by a factor of  $1/Z_{\text{rot}} = 0.26$  at  $T = 400$  K. Considering that each molecule can perform up to  $g_j = 4$  equivalent jumps of length  $l_j = 2.35$  Å, we arrive at a diffusivity represented by the red line with label 1 in Figure 8, which underestimates the measured



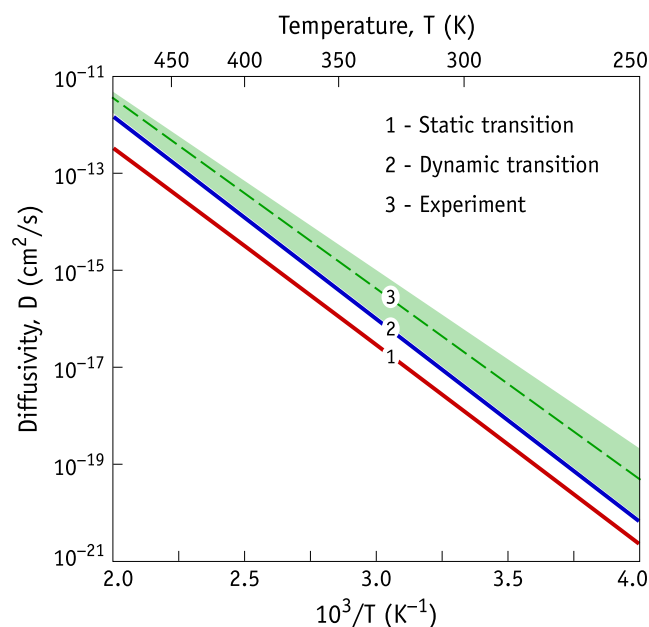


**Figure 8.** Diffusivity of molecular hydrogen in silicon. The red and blue solid lines (1 and 2) represent the calculated diffusivity of  $H_{2T}$  assuming a static and dynamic (free rotor) molecule at the transition state, respectively. An Arrhenius plot obtained from measurements in the temperature range  $T = 300 - 420$  K<sup>[35]</sup> is also shown (green dashed line 3). The shadow green area limits the upper and lower bounds of the measured diffusivity of the molecule as estimated from the error bars of the pre-exponential and energy barrier from the fit.

diffusivity (dashed green line with label 3) by a factor of 10 in the temperature range  $T = 300 - 400$  K.

If, on the other hand, we consider a dynamic transition state,  $\nu_0$  is not reduced and we arrive at a calculated diffusivity of  $D = (3.4 \times 10^{-4} \text{ cm}^2 \text{ s}^{-1}) \exp(-0.82 \text{ eV} / k_B T)$ . This result is shown in Figure 8 as a solid blue line with label 2, edging the lower bound of the experimental values (considering their respective errors).<sup>[35]</sup> The calculated prefactor of the dynamic transition mechanism overestimates the measured figure by a factor of 1.3 only (see Table 1). These results, along with the flat potential for rotation of the molecule at the saddle point, suggest that the  $H_{2T}$  molecules not only rotate freely on their stable sites, but they also rotate during migration.

## 4. Conclusions

We presented a theoretical study of the dynamics of atomic hydrogen and hydrogen dimers in silicon at finite temperatures. Hybrid density functional theory was employed to obtain the electronic (plus clamped ionic) potential and activation barriers for migration/reconfiguration. Semilocal density functional theory was used to calculate vibrational frequencies within the harmonic approximation. Besides the potential energy, we calculated free energies which account for vibrational, rotational, and configurational degrees of freedom within a diluted regime.

For the sake of convenience, we collected all calculated properties pertaining atomic hydrogen defects ( $H_{BC}^+$ ,  $H_{BC}^0$ ,  $H_{AB}^0$ , and

$H_{AB}^-$ ) and stable hydrogen dimers ( $H_2^*$  and the  $H_{2T}$  molecule) in Table 1. Here, one can find the configurational degeneracy per unit cell for each defect ( $g$ ), some bond lengths ( $d$ ), zero-phonon energies ( $\Delta E_{ZP}$ ), activation energies for migration and reconfiguration ( $\Delta E_a$ ), their respective attempt frequencies ( $\nu_0$ ), jumping degeneracy ( $g_j$ ), jump distance ( $l_j$ ), reconfiguration and carrier emission energies ( $\Delta E$  is positive/negative for endo-thermic/exothermic processes), diffusivity prefactors ( $D_0$ ), and LVM frequencies (above the Raman edge). Several quantities can be compared directly with experimental values (rightmost column).

In the first part of Section 3, we reproduced the well-established negative- $U$  model of atomic hydrogen in Si, involving a metastable neutral state that disproportionates into stable bond-centered (positively charged) or antibonding (negatively charged) species. The transition between the stable states is estimated to occur when the Fermi level crosses  $E(-/+)=E_c-0.30$  eV. Metastable transition levels at  $E(0/+)=E_c-0.20$  eV and  $E(-/0)=E_c-0.61$  eV were found for the  $H_{BC}$  and  $H_{AB}$  species, respectively, and they compare fairly well with the experimental findings.

The zero-point energy contribution to the calculated transition energies is not negligible. For  $H_{BC}$ , this quantity differs from that of  $H_{AB}$  by about 0.1 eV. Due to cancellation effects, the impact of zero-point motion on the calculated transition energies involving identical configurations is minor. However, the  $(-/0)$  and  $(-/ +)$  levels involving  $H_{AB}^- \rightarrow H_{BC}^0 + e^-$  and  $H_{AB}^- \rightarrow H_{BC}^+ + 2e^-$  are affected by errors of 0.1 and 0.05 eV, respectively, when zero-point motion is not considered.

Regarding the formation mechanism of hydrogen molecules in Si quenched from high temperatures ( $T \gtrsim 700^\circ\text{C}$ ), we found the following.

The calculated migration barrier of the molecule is about 0.8 eV. This figure is very close to the measured value and it is consistent with the observation of mobile molecules just above room temperature.<sup>[35]</sup>

Based on the calculated attempt rate and barrier for dissociation of the molecule (transformation into  $H_2^*$ ), the annealing temperature of  $H_{2T}$  was estimated as  $T \approx 700$  K. This is an upper bound as it neglects trapping by and reaction with defects. Nevertheless, these results suggest that the lifetime of  $H_{2T}$  significantly exceeds that of  $H_2^*$  (which according to the experimental results is not thermally stable above  $200^\circ\text{C}$ <sup>[27]</sup>). Even up to this temperature, when formation of  $H_2^*$  can compete with that of  $H_{2T}$ , the molecule is invariably more stable, and that relative stability increases with temperature. The free energy of formation of the molecule is 0.2 and 0.4 eV lower than that for  $H_2^*$  at  $T = 0$  and 500 K, respectively. We could not find any other H dimer, which could be considered stable enough as to compete with the formation of  $H_{2T}$  and  $H_2^*$ .

Due to configurational entropy, the stability of H monomers increases with temperature. However, the relative stability of antibonding monomers, especially the negatively charged  $H_{AB}^-$  state, increases faster with temperature, and therefore  $H_{AB}^-$  becomes the second most stable monomer after  $H_{BC}^+$  above 500 K. We estimate that at  $T \approx 1200^\circ\text{C}$ , the free energy of  $H_{AB}^-$  is only 0.12 eV above  $H_{BC}^+$ , and its population is nearly 1/4 of the total free hydrogen.

We propose the following stages for the condensation of atomic H into molecules during cooling: 1) above  $T \approx 700$  K, the molecules are not stable and free hydrogen may only be found in the atomic form, mostly as  $H_{BC}^+$ , but also as a small fraction of  $H_{AB}^-$ . 2) In the temperature window  $T \approx 700 - 500$  K, the Coulomb interaction between  $H_{BC}^+$  and a small population of  $H_{AB}^-$  leads to the formation stable  $H_{2T}$  molecules. At this point, no other dimers are stable. 3) Below  $T \approx 500$  K, the fraction of  $H_{AB}^-$  becomes negligible in comparison to other states, effectively stopping further formation of molecules.

The above also explains why it is so difficult to form  $H_2^*$  in quenched material, despite its considerable stability compared to the molecule.

The formation of  $H_{AB}^-$  could also partially explain the apparent inconsistency between the high-temperature and low-temperature diffusivity of atomic hydrogen in Si. While the description of the low-temperature diffusivity of the dominant  $H_{BC}^+$  state is acceptable, in the range  $T = 1300 - 1500$  K the calculated  $H_{BC}^+$  diffusivity is lower compared to the experimentally determined values by a factor of 20. Adding the contribution to the diffusivity from the  $H_{AB}^-$  population increased the effective diffusivity by a factor of 3. However, the larger enhancement occurred when we took into account a thermal population of fast-diffusing  $H_{AB}^0$  species. At such high temperatures, the free energy of this state is close to that of  $H_{BC}^0$  and their concentrations are also comparable. However, the minute barrier for migration of  $H_{AB}^0$  ( $\Delta E_a \approx 40$  meV) increases the effective diffusivity by a factor of 10, further narrowing the discrepancy between the calculated and experimentally determined values.

Finally, unlike the commonly pictured mechanism for the migration of molecular hydrogen in Si, according to which  $H_{2T}$  jumps between neighboring T sites with their H—H bond perpendicular to the hexagonal rings of the Si crystal, we found that the potential energy change for molecular rotation at the saddle point is only a few meV. We also found that the observed diffusivity of the molecule is better described if it migrates as a nearly free rotor, all along the minimum energy path, including at the transition state.

## Acknowledgements

This work was supported by the FCT in Portugal through Projects UID-B/50025/2020, UID-P/50025/2020, and 2021.09643.CPCA (Advanced Computing Project using the Oblivion supercomputer). The work in the UK was funded by EPSRC via grant EP/TO25131/1. J.C. acknowledges Dr. Vladimir Voronkov for fruitful discussions regarding the diffusivity of atomic hydrogen.

## Conflict of Interest

The authors declare no conflict of interest.

## Data Availability Statement

The data that support the findings of this study are available from the corresponding author upon reasonable request.

## Keywords

defects, hydrogen, molecules, silicon, thermodynamics

Received: December 30, 2021

Revised: February 7, 2022

Published online: March 16, 2022

- [1] *Hydrogen in Semiconductors: Bulk and Surface Properties* (Eds: M. Stutzmann, J. Chevallier), Elsevier, Amsterdam **1991**.
- [2] *Hydrogen in Semiconductors* (Eds: J. I. Pankove, N. M. Johnson), Semiconductors and Semimetals, Vol. 34, Academic Press, Boston **1991**.
- [3] S. J. Pearton, J. W. Corbett, M. Stavola, in *Springer Series in Materials Science* Vol. 16, Springer Verlag, Berlin, **1992**.
- [4] *Hydrogen In Semiconductors II* (Ed: N. Nickel), Semiconductors and Semimetals, Vol. 61, Academic Press, San Diego **1999**.
- [5] A. R. Peaker, V. P. Markevich, L. Dobaczewski, in *Defects in Microelectronic Materials and Devices*, CRC Press, Boca Raton, FL, **2008**, Ch. 2, pp. 27–55.
- [6] S. K. Estreicher, M. Stavola, J. Weber, in *Silicon, Germanium, and Their Alloys: Growth, Defects, Impurities, and Nanocrystals*, CRC Press, Boca Raton, **2014**, Ch. 7, 217–254.
- [7] B. B. Nielsen, K. B. Nielsen, J. P. Byberg, *Mater. Sci. Forum* **1994**, 143–147 909.
- [8] Y. V. Gorelinskii, N. N. Nevinnyi, *Mater. Sci. Eng., B* **1996**, 36, 133.
- [9] C. A. J. Ammerlaan, P. T. Huy, *Solid State Phenom.* **2002**, 85–86 353.
- [10] N. M. Johnson, C. Herring, C. G. Van de Walle, *Phys. Rev. Lett.* **1994**, 73, 130.
- [11] K. B. Nielsen, B. B. Nielsen, J. Hansen, E. Andersen, J. U. Andersen, *Phys. Rev. B* **1999**, 60, 1716.
- [12] M. Budde, G. Lüpke, C. P. Cheney, N. H. Tolk, L. C. Feldman, *Phys. Rev. Lett.* **2000**, 85, 1452.
- [13] B. Hitti, S. R. Kreitzman, T. L. Estle, E. S. Bates, M. R. Dawdy, T. L. Head, R. L. Lichti, *Phys. Rev. B* **1999**, 59, 4918.
- [14] T. Sasaki, H. Katayama-Yoshida, *J. Phys. Soc. Jpn.* **1989**, 58, 1685.
- [15] C. G. Van de Walle, P. J. H. Denteneer, Y. Bar-Yam, S. T. Pantelides, *Phys. Rev. B* **1989**, 39, 10791.
- [16] R. Jones, *Physica B: Condens. Matter* **1991**, 170, 181.
- [17] C. Herring, N. M. Johnson, C. G. Van de Walle, *Phys. Rev. B* **2001**, 64, 125209.
- [18] B. Hourahine, R. Jones, S. Öberg, P. R. Briddon, T. Frauenheim, *J. Phys.: Condens. Matter* **2003**, 15, S2803.
- [19] S. K. Estreicher, A. Docaj, M. B. Bebek, D. J. Backlund, M. Stavola, *Phys. Status Solidi A* **2012**, 209, 1872.
- [20] S. Z. Karazhanov, M. Ganchenkova, E. S. Marstein, *Chem. Phys. Lett.* **2014**, 601 49.
- [21] G. D. Watkins, in *Advances in Solid State Physics*, Vol. 24 (Ed: P. Grosse), Springer, Berlin, Heidelberg **1984**, pp.163–189.
- [22] J. Coutinho, V. P. Markevich, A. R. Peaker, *J. Phys.: Condens. Matter* **2020**, 32, 323001.
- [23] K. B. Nielsen, L. Dobaczewski, S. Søgård, B. B. Nielsen, *Phys. Rev. B* **2002**, 65, 075205.
- [24] A. V. Wieringen, N. Warmoltz, *Physica* **1956**, 22, 849.
- [25] Y. Kamiura, M. Yoneta, F. Hashimoto, *Appl. Phys. Lett.* **1991**, 59, 3165.
- [26] M. J. Binns, S. A. McQuaid, R. C. Newman, E. C. Lightowlers, *Semicond. Sci. Technol.* **1993**, 8, 1908.
- [27] J. D. Holbeck, B. B. Nielsen, R. Jones, P. Sitch, S. Öberg, *Phys. Rev. Lett.* **1993**, 71, 875.
- [28] S. K. Estreicher, M. Sanati, D. West, F. Ruymgaart, *Phys. Rev. B* **2004**, 70, 125209.

- [29] M. Suezawa, *Jpn. J. Appl. Phys.* **1999**, 38, 5A L484.
- [30] S. K. Estreicher, J. L. Hastings, P. A. Fedders, *Phys. Rev. Lett.* **1999**, 82, 815.
- [31] T. Ichimiya, A. Furuichi, *Int. J. Appl. Radiat. Isotopes* **1968**, 19, 573.
- [32] V. V. Voronkov, R. Falster, *Phys. Status Solidi B* **2017**, 254, 1600779.
- [33] A. W. R. Leitch, V. Alex, J. Weber, *Phys. Rev. Lett.* **1998**, 81, 421.
- [34] R. E. Pritchard, M. J. Ashwin, J. H. Tucker, R. C. Newman, *Phys. Rev. B* **1998**, 57, R15048.
- [35] V. P. Markevich, M. Suezawa, *J. Appl. Phys.* **1998**, 83, 2988.
- [36] C. Peng, H. Zhang, M. Stavola, W. B. Fowler, B. Esham, S. K. Estreicher, A. Docaj, L. Cernel, M. Seacrist, *Phys. Rev. B* **2011**, 84, 195205.
- [37] R. E. Pritchard, J. H. Tucker, R. C. Newman, E. C. Lightowers, *Semicond. Sci. Technol.* **1999**, 14, 77.
- [38] O. Andersen, A. R. Peaker, L. Dobaczewski, K. B. Nielsen, B. Hourahine, R. Jones, P. R. Briddon, S. Öberg, *Phys. Rev. B* **2002**, 66, 235205.
- [39] J. M. Pruneda, S. K. Estreicher, J. Junquera, J. Ferrer, P. Ordejón, *Phys. Rev. B* **2002**, 65, 075210.
- [40] B. Hourahine, R. Jones, S. Öberg, R. C. Newman, P. R. Briddon, E. Roduner, *Phys. Rev. B* **1998**, 57, R12666.
- [41] V. V. Voronkov, R. Falster, *Phys. Status Solidi A* **2017**, 214, 1700287.
- [42] N. M. Johnson, C. Herring, *Phys. Rev. B* **1992**, 46, 15554.
- [43] S. K. Estreicher, C. H. Seager, R. A. Anderson, *Appl. Phys. Lett.* **1991**, 59, 1773.
- [44] K. Ramspeck, S. Zimmermann, H. Nagel, A. Metz, Y. Gassenbauer, B. Birkmann, A. Seidl, in *Proc. of the 27th European Photovoltaic Solar Energy Conf.*, WIP, München, **2012**.
- [45] D. Chen, M. V. Contreras, A. Ciesla, P. Hamer, B. Hallam, M. Abbott, C. Chan, *Progr. Photovolt. Res. Appl.* **2020**, 29, 1180.
- [46] J. A. T. D. Guzman, V. P. Markevich, J. Coutinho, N. V. Abrosimov, M. P. Halsall, A. R. Peaker, *Sol. RRL* **2021**, 2100459.
- [47] C. Sun, F. E. Rougieux, D. Macdonald, *J. Appl. Phys.* **2015**, 117, 045702.
- [48] C. Sun, D. Yan, D. Macdonald, *Phys. Status Solidi RRL* **2021**, 15, 2100483.
- [49] G. Kresse, J. Hafner, *Phys. Rev. B* **1993**, 47, 558.
- [50] G. Kresse, J. Hafner, *Phys. Rev. B* **1994**, 49, 14251.
- [51] G. Kresse, J. Furthmüller, *Phys. Rev. B* **1996**, 54, 11169.
- [52] G. Kresse, J. Furthmüller, *Comput. Mater. Sci.* **1996**, 6, 15.
- [53] J. P. Perdew, K. Burke, M. Ernzerhof, *Phys. Rev. Lett.* **1996**, 77, 3865.
- [54] J. Heyd, G. E. Scuseria, M. Ernzerhof, *J. Chem. Phys.* **2003**, 118, 8207.
- [55] J. Heyd, G. E. Scuseria, M. Ernzerhof, *J. Chem. Phys.* **2006**, 124, 219906.
- [56] P. E. Blöchl, *Phys. Rev. B* **1994**, 50, 17953.
- [57] C. Freysoldt, J. Neugebauer, C. G. Van de Walle, *Phys. Rev. Lett.* **2009**, 102016402.
- [58] G. Henkelman, B. P. Uberuaga, H. Jónsson, *J. Chem. Phys.* **2000**, 113, 9901.
- [59] H. J. Monkhorst, J. D. Pack, *Phys. Rev. B* **1976**, 13, 5188.
- [60] D. Murali, M. Posselt, M. Schiwarth, *Phys. Rev. B* **2015**, 92, 064103.
- [61] O. K. Al-Mushadani, R. J. Needs, *Phys. Rev. B* **2003**, 68, 235205.
- [62] X. Zhang, B. Grabowski, T. Hickel, J. Neugebauer, *Comput. Mater. Sci.* **2018**, 148, 249.
- [63] Y. Mishin, M. R. Sørensen, A. F. Voter, *Philos. Mag. A* **2001**, 81, 2591.
- [64] S. Huang, D. L. Worthington, M. Asta, V. Ozolins, G. Ghosh, P. K. Liaw, *Acta Mater.* **2010**, 58, 1982.
- [65] N. W. Ashcroft, N. D. Mermin, *Solid State Physics*, Saunders College Publishing, New York **1976**.
- [66] P. Flubacher, A. J. Leadbetter, J. A. Morrison, *Philos. Mag.* **1959**, 4, 273.
- [67] P. D. Desai, *J. Phys. Chem. Ref. Data* **1986**, 15, 967.
- [68] S. K. Estreicher, K. Wells, P. A. Fedders, P. Ordejón, *J. Phys.: Condens. Matter* **2001**, 13, 6271.
- [69] E. V. Lavrov, J. Weber, *Phys. Rev. Lett.* **2002**, 89, 215501.
- [70] G. Colonna, A. D'Angola, M. Capitelli, *Int. J. Hydrog. Energy* **2012**, 37, 9656.
- [71] G. H. Vineyard, *J. Phys. Chem. Solids* **1957**, 3, 121.
- [72] P. Hänggi, P. Talkner, M. Borkovec, *Rev. Mod. Phys.* **1990**, 62, 251.
- [73] L. T. Kong, L. J. Lewis, *Phys. Rev. B* **2006**, 74, 073412.
- [74] C. P. Herrero, *Phys. Rev. B* **1997**, 55, 9235.
- [75] C. G. Van de Walle, Y. Bar-Yam, S. T. Pantelides, *Phys. Rev. Lett.* **1988**, 60, 2761.
- [76] K. Irmscher, H. Klose, K. Maass, *J. Phys. C: Solid State Phys.* **1984**, 17, 6317.
- [77] C. G. Van de Walle, J. Neugebauer, *Nature* **2003**, 423, 626.
- [78] N. Fujimura, A. Ohta, K. Makiyama, S. Miyazaki, *Jpn. J. Appl. Phys.* **2016**, 55, 08PC06.
- [79] B. Hourahine, *Ph.D. Thesis*, University of Exeter, **2000**.
- [80] M. Budde, C. P. Cheney, G. Lüpke, N. H. Tolk, L. C. Feldman, *Phys. Rev. B* **2001**, 63, 195203.